Available online at www.sciencedirect.com
SCIENCE DIRECT
Carbon 44 (2006) 2178–2183
CARBON
www.elsevier.com/locate/carbon

High-temperature electrical transport properties of buckypapers composed of doped single-walled carbon nanotubes

Sławomir Kulesza [a,*], Paweł Szroeder [a], Jaromir K. Patyk [a], Janusz Szatkowski [a], Marcin Kozanecki [b]

[a] Instytut Fizyki, Uniwersytet Mikołaja Kopernika, Grudziądzka 5/7, 87-100 Toruń, Poland
[b] Katedra Fizyki Molekularnej, Politechnika Łódzka, Żeromskiego 116, 90-924 Łódź, Poland

Received 3 July 2005; accepted 9 March 2006
Available online 2 May 2006

Abstract

Data on temperature-dependent electrical resistance of buckypaper flakes are presented in this paper. The buckypapers are composed of ropes of aligned single-walled carbon nanotubes doped with HNO_3, which are treated as mixed systems with their properties being dependent on the treatment performed. The measurements cover rather wide temperature range from 300 up to 900 K. In case of untreated samples, curves with two well-defined activation energies are seen, which are discussed in terms of different DC conductivity mechanisms, with a great attention paid to the parallel metal-semiconductor system. In turn, in heat-treated samples the resistance is found nearly temperature-independent except for the significant peak centered at about 600–650 K. Observed characteristics are also fitted using the parallel model, although with a less accuracy suggesting influence of another conductivity mechanisms. At any rate, the resistance peak is possibly related to the metal/non-metal transition observed in disordered solids.

Keywords: Carbon nanotubes; Electrical properties

1. Introduction

In the first approximation, carbon nanotubes (CNTs) may exhibit either semimetallic or semiconducting properties depending on their chirality and diameter [1]. This is because the conformation of the tubes strongly affects their intrinsic properties. On the other hand, extrinsic electrical properties of CNTs have been found significantly sensitive to adsorption including, for instance, the effect of oxygen [2] and water vapor [3]. Similar to graphite, structural distortions caused by exohedral doping with alkali metal atoms (K, Br) are known to modify the charge carrier transport as well [4]. Another way to modify the electrical conductivity of CNTs is possible thanks to the substitutional doping, i.e., incorporation of foreign atoms (N, B) directly into lattice sites [5].

Carbon nanotubes reveal quantum transport phenomena at low-temperatures [6]. On the other hand, nanotube-based devices are required to handle at moderate temperatures from 300 up to 500 K typically, and within this range the electrical transport mechanisms are quite well described [7]. At higher temperatures, however, these mechanisms are considered mostly speculative due to the lack of measurements performed so far. Present paper aims at casting some light into this issue dealing with large structures composed of dense-packed single-wall carbon nanotubes, namely the so-called buckypapers.

2. Experimental

Single-walled carbon nanotubes have been produced by means of the DC-arc discharge method [8–11]. A tubular

* Corresponding author. Tel.: +48 56 611 32 52; fax: +48 56 622 53 97.
E-mail address: colage@phys.uni.torun.pl (S. Kulesza).

0008-6223/$ - see front matter © 2006 Elsevier Ltd. All rights reserved.
doi:10.1016/j.carbon.2006.03.012

quartz chamber as long as 400 and 50 mm in diameter with a pair of electrodes placed vertically has been used. In such a configuration, the graphitic cathode was mounted over the anode that was made of graphite and capped with a pellet containing graphite admixed with 0.6 at.% of nickel and 0.6 at.% of yttrium catalyst powders. During the discharge sustained by the current of 50 A at a voltage of 21 V, the pellet underwent an evaporation. The synthesis was carried out in helium-rich atmosphere under pressure of 66 kPa (500 Tr) with the gas flow of 500 sccm. The discharge region was additionally heated up to 770 K.

Soot with nanotubes was collected from the inner walls of the quartz tube, above the discharge region. In order to dope nanotubes in the soot and to eliminate the undesirable admixture of catalyst nanoparticles, the soot was treated with 3 M aqueous solution of nitric acid at 110 °C for 20 h, followed by the settlement of the obtained suspension for another 24 h. Then the nitric acid solution was poured out and the remaining soot was rinsed with distilled water. This operation was subsequently repeated three times. To remove residual liquid particles, the suspension was drawn through the ceramic filter resulting in a uniform black deposit. Once dried, the deposit turned into shiny gray structure referred to as buckypaper.

Raman spectra of the SWNT films were measured with Jobin–Yvone T64000 triple Raman system. In turn, DC electrical characteristics were measured in a flat configuration using Keithley 6517 electrometer with a 2-point contact probe made of platinum wires. Temperature-dependent characteristics of the resistance in vacuum of 0.13 Pa (10^{-3} Tr) were probed at low applied voltage of 0.1 V (ohmic contact regime). The temperature increased at a constant rate of 2 K/min up to 900 K during measurements.

In advance of that, however, simple procedure has been used to verify that observed resistance was actually due to the buckypaper rather than interface contacts. To this end, a series of resistance measurements with the varied probe spacing has been carried out at room temperature. Then, the plot of the resistance against the probe distance has been fitted with the linear function, as shown on the left upper inset of Fig. 3, extrapolation of which down to the *y*-intercept yielded the contact resistance as low as 200 Ω. Obtained value was about 10 times smaller than the resistance at the probe spacing of 1 mm used for the DC measurements throughout this study. Therefore, the measured resistance has been proved to be dominated by the nanotube network with only small contribution of the contact interface.

3. Results and discussion

The micro-Raman spectra of the buckypapers recorded at two different laser wavelengths, namely 632.8 nm (1.96 eV) and 514.5 nm (2.41 eV), are shown in Fig. 1. There are selectively induced Raman peaks in the range of 145–180 cm^{-1} that are attributed to the so-called radial breathing modes (RBM) of SWNTs [12]. Analysis of these

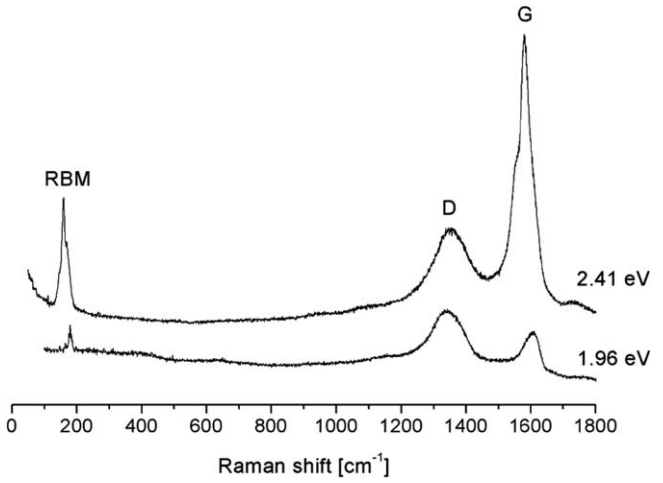

Fig. 1. Micro-Raman spectra of the buckypaper excited with laser wavelengths of 514.5 (top) and 632.8 nm (bottom) corresponding to photon energies of 2.41 and 1.96 eV, respectively.

modes using the Kataura plot shows clearly the presence of semiconducting tubes with the 2.41 eV excitation line, but only a small amount of metallic tubes with the 1.96 eV excitation line. Such predominance of semiconducting SWNTs over metallic ones stems from the procedure of purification of the raw material, due to which boiling in nitric acid, apart from removing metal particles, introduces structural defects into the tubes. On the other hand, peaks centered at 1350 and 1580 cm^{-1} referred to as *D*-line and *G*-line, respectively, are characteristic of Raman scattering in sp^2 carbon phase.

According to the SEM image in Fig. 2, the buckypapers are flake-like structures with bent edges. Their uneven surface is intersected by numerous cracks of the width varying from hundreds nanometers up to tens micrometers. Such a structure is assumed to be the conductive network, i.e., the ensemble of semiconducting SWNTs interconnected into a

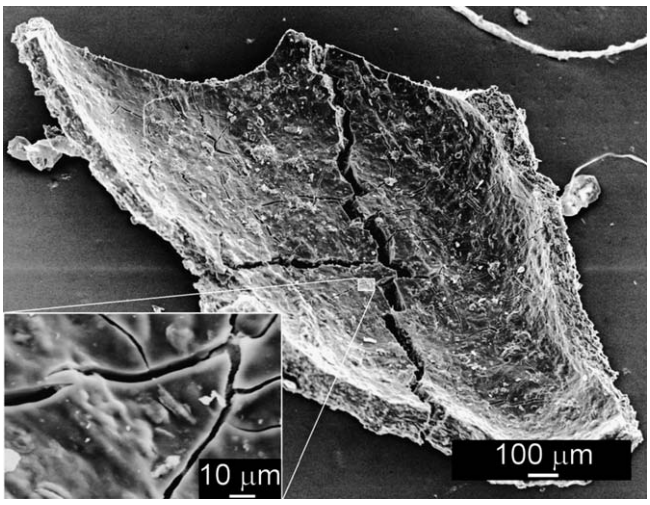

Fig. 2. SEM image of the buckypaper sample exhibiting flake-like shape with bent edges.

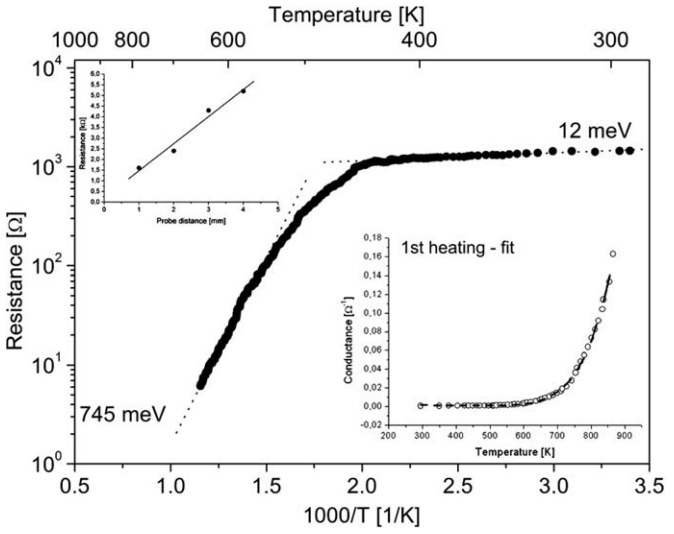

Fig. 3. Arrhenius plot of the temperature-dependent electrical resistance of the buckypaper sample. The two distinct regimes of the electrical conductivity are observed: 12 meV at moderate temperatures, and 745 meV at high-temperatures. Insets: the resistance vs. probe distance plot used to estimate the contribution of the contact resistance to the overall resistance (upper left); the fit of the parallel resistance model to $1/R$ (conductance) data (bottom right).

percolating system, for which there have been several electron transport models developed so far [13–16]. This is, because any electron on its path along the fibres encounters a number of defects, inter-tube as well as inter-bundle contacts, geometrical deformations, etc., which serve actually as barriers. Only the case of an individual SWNT as well as a highly ordered bundle, in which every single nanotube represents a simple bridge between the point-probe electrodes, is excluded from the analysis given in the following paragraphs.

An example of the temperature-dependent resistance of the untreated buckypaper sample in vacuum is drawn in Fig. 3. Apparently, two temperature limits are seen in this case. In the low-temperature limit ($T \approx T_{\mathrm{room}}$) the resistance is found to approach the asymptote, i.e., it changes with very low activation energy of 12 meV, whereas in the high T limit ($T \to 900$ K) the resistance falls down more rapidly being governed by the activation energy of 745 meV. Such a behavior has been found reproducible, i.e., repeated measurements within a set of six samples gave similar results: the mean value of the low-temperature activation energy is 25 ± 5 meV, while the high-temperature one is 770 ± 90 meV. As a matter of fact, the mean low-temperature activation energy equals to that of thermal vibrations of the lattice at room temperature pointing at some curiosity in the conductivity, but this seems to be an intrinsic property of the system. In the following, those energies are discussed in terms of the most important parameters of disordered systems.

Bernasconi [16] has analyzed hopping transport in disordered classical-resistance network in the form of two- or three-dimensional regular lattice, nodes of which were connected by temperature-dependent conductances $\sigma_{\mathrm{i}} = \sigma_0 \times \exp(-\beta E_{\mathrm{i}})$, $\beta = (kT)^{-1}$. What was important, activation energies E_{i} were distributed according to the probability density $\rho(E)$. It was found, that in the small-β limit, conductivity was simply given by:

$$\ln\left(\frac{\sigma}{\sigma_0}\right) \approx -\beta E^{(0)} \tag{1}$$

where

$$E^{(0)} = \langle E \rangle = \int \rho(E) \cdot E \cdot \mathrm{d}E \tag{2}$$

On the other hand, in the large-β limit:

$$\ln\left(\frac{\sigma}{\sigma_\infty}\right) \approx -\beta E^{(\infty)} \tag{3}$$

with the activation energy $E^{(\infty)}$ being related to the percolation threshold p_{c} as follows:

$$\int_{-\infty}^{E^{(\infty)}} \rho(E) \cdot \mathrm{d}E = p_{\mathrm{c}} \tag{4}$$

Assuming the uniform distribution $\rho(E) = 1/E_{\mathrm{m}}$, $0 \leqslant E \leqslant E_{\mathrm{m}}$, critical-path analysis led to:

$$E^{(\infty)} = p_{\mathrm{c}} \cdot E_{\mathrm{m}} \tag{5}$$

$$E^{(0)} = \frac{1}{2} E_{\mathrm{m}} \tag{6}$$

Having established the percolation model, activation energies given in Fig. 3 result in: $E_{\mathrm{m}} = 1.49$ eV, and $p_{\mathrm{c}} = 0.008$, which in the following yielded unrealistic coordination number of the three-dimensional lattice $z = 186$.

Similar results were obtained using the effective-medium approach, according to which (same uniform energy distribution):

$$E^{(0)} = \langle E \rangle \tag{7}$$

$$E^{(\infty)} = \frac{2}{z} E_{\mathrm{m}} \tag{8}$$

Here, even higher coordination number $z = 248$ corresponded to given activation energies. Let us take the notice, however, that simulated functions fit experimental curves very well, and hence the origin of such unrealistic coordination numbers needs to be examined in further work. One of possible directions would involve using more sophisticated energy distribution function.

A second approach takes advantage of a temperature-dependent model of the conductivity developed for dirty metals. In such a case, the conductance (reciprocal resistance R) is expressed in the simple power-law form [17]:

$$[R(T)]^{-1} = A + B \cdot T^C \tag{9}$$

where T is the temperature, while A, B, and C – fitted parameters. A least-squares fit (not shown), although numerically reasonable ($\chi^2 < 10^{-5}$), yields A and B close to zero, and the exponent $C \approx 10$. On the basis of theory of dirty metals, however, the exponent is expected not to be greater than two having the linear coefficient B been negative. Observed inconsistency with the data might

probably arise from the fact that the validity of the model is limited to very low-temperatures regime and it would break down when extrapolated to higher temperatures.

Alternatively, $R(T)$ data could be also examined in the frame of more complex models that have been proposed, for instance, for fibrillar polymers. Such polymers are composed of single polymer chains aligned with each other over the length of 10–50 nm to form ordered crystallites, which in the following are interconnected by amorphous regions [15]. Their similarity to the buckypaper discussed in this paper follows from the fact that ordered fibres correspond to bundles of nanotubes in the buckypaper, whereas amorphous regions correspond to shape deformations, intertube contacts, and defects in the buckypaper, all of which play the role of barriers to conduction. Although a plenty of series resistance models have been proposed for the SWNT mats, the best fit was obtained for a simple sum of standard metallic transport and fluctuation-assisted tunnelling between metallic regions [18]:

$$R(T) = A \cdot T + B \cdot \exp[C/(T + D)] \tag{10}$$

where R describes the measured resistance, T – the temperature, whereas A, B, C, and D – fitted parameters. According to this model, however, it is the metallic term which is expected to dominate at higher temperatures, and hence the fitting procedure would fail with respect to our data. On the other hand, the best fit to the curve in Fig. 3 have been found using a parallel resistance model, in which the tunnelling term is replaced by a thermally-activated exponential decay in the form:

$$[R(T)]^{-1} = A/T + B \cdot \exp[-C/T] \tag{11}$$

where A, B, and C are the parameters. Given semiconducting contribution increases with the temperature and at sufficiently high temperature becomes dominant over the metallic term. The inset of Fig. 3 (bottom right) shows the reciprocal resistance data from Fig. 3 plotted as a function of the absolute temperature together with the best fit obtained using the expression (11). According to that, the linear resistance coefficient $\alpha = 1/A = 2.15\ \Omega/\mathrm{K}$ (metallic contribution), asymptotic resistance $R_\infty = 1/B = 3.3 \times 10^{-4}\ \Omega$, and activation energy $E_A = k \times C = 737$ meV. Let us notice that obtained activation energy is in excellent agreement with that observed in Fig. 3 in the high-temperature limit, which actually supports the semiconducting contribution to the DC conductivity of the buckypaper.

Resistance against temperature characteristics of the same sample subjected to recurrent heat treatment in vacuum are shown in Fig. 4. The data have been taken subsequently to that in Fig. 3 without any exposure of the sample to gas species in the meantime. Again, at moderate temperatures the curve following flat line is evident pointing at metallic-like behavior of the buckypaper (zero activation energy). At higher temperatures, however, significant peak of resistance centered at about 650 K turns out. Here, the plot extends over seven orders of magnitude and then the resistance falls down back to its initial value. The curve

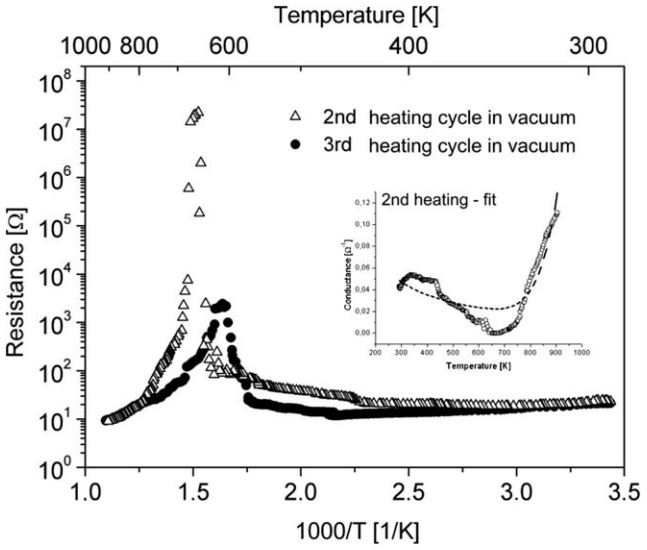

Fig. 4. Arrhenius plots of the electrical resistance against temperature of the buckypaper sample measured during the second and third recurrent heat treatment cycles in vacuum without any exposure to gas species in the meantime. Inset: the fit of the parallel resistance model to conductance data of the second heating cycle.

observed during the third heating cycle is weaker in comparison with the previous one in the same figure, and is additionally shifted down to 600 K.

The parallel resistance characteristics (11) have been also used to fit the resistance from Fig. 4, and the inset of Fig. 4 shows an example of the fit. In terms of the model, the resistance characteristics peak appears when the non-metallic transport mode brings the dominant contribution to the DC conductivity at the expense of the metallic conductivity. Numerical fit yields the following parameters: activation energy $E_A = 993$ and 827 meV for the second and the third heating cycle, respectively, asymptotic resistance $R_\infty = 2.6 \times 10^{-5}$ and $2.6 \times 10^{-4}\ \Omega$, the linear resistance coefficient $\alpha = 7.1 \times 10^{-2}$ and $5.7 \times 10^{-2}\ \Omega/\mathrm{K}$. In general, however, the fitting procedure tends to be less accurate with increasing number of the annealing cycles, which strongly suggests metastable character of the DC conductivity observed in the buckypaper.

According to Fig. 5, it would be the alignment effect caused by the annealing which is likely to decrease the room temperature resistance of the annealed structure in comparison with its as-prepared state. The tubes having been oriented almost parallel, even small fraction of metallic SWNTs might dominate the $R(T)$ curve. Such effect, shown in Fig. 5 where TEM images of the buckypaper before- and after vacuum annealing at 900 K are presented, might be further enhanced by de-doping of semiconducting tubes. According to ESR measurements (not shown), the electrical conductivity of individual tubes increases by a factor of 20 after annealing with respect to the as-prepared material [19]. Such a result seems to agree strikingly with the fit, where the asymptotic resistance R_∞ fell down from 3.3×10^{-4} to $2.6 \times 10^{-5}\ \Omega$ after annealing.

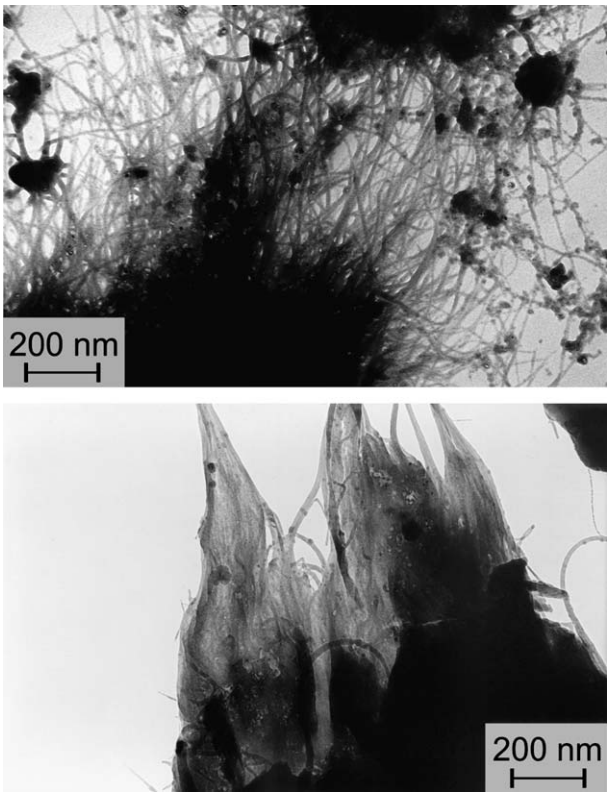

Fig. 5. TEM images of the buckypaper sample recorded in the as-prepared state (upper), and after the vacuum annealing treatment at 900 K (bottom). The annealing results in substantial alignment of the tubes in the sample.

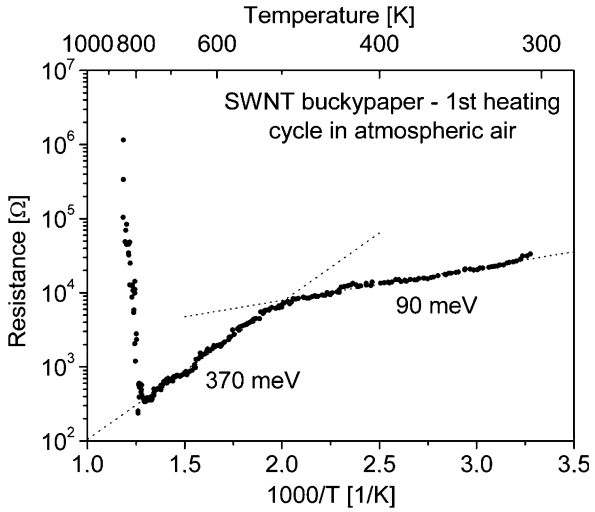

Fig. 6. The surface resistance against temperature characteristics of the buckypaper sample exposed to atmospheric air, drawn in the form of Arrhenius plot.

In Fig. 6, temperature-dependent plot of the resistance measured under atmospheric air is shown. As in Fig. 3, the curve splits up into two distinct parts. The first one at moderate temperatures of 300-500 K corresponds to the activation energy of 90 meV, which is markedly higher than that in Fig. 3, while in the second one (500–800 K) the activation energy increases up to 370 meV. The latter activation energy is consistent with that obtained by using the parallel resistance model ($E_A = 399$ meV, the asymptotic resistance $R_\infty = 0.93\ \Omega$, and the linear resistance coefficient $\alpha = 53\ \Omega/K$). At temperatures higher than 800 K, however, the curve rapidly goes upwards due to complete oxidation of the material followed by its evaporation. Unfortunately, complete vaporization of the sample at 800 K in the air made impossible further studies that include the same recurrent heat treatment procedure as for vacuum-annealed sample.

To sum up, data on electrical resistance of SWNTs contained in the buckypapers measured in the temperature range extending from 300 up to 900 K are presented in this paper. The regular curves with well-defined activation energies are observed for the samples not subjected to any heat treatment, which are discussed in terms of various DC conductivity models. In contrast, almost temperature-independent $R(T)$ characteristics are found in case of heat-treated samples containing noticeable resistance peak at 600–650 K. Such a peak is presumably attributed to metal–non-metal transition observed in mixed crystalline-amorphous systems. Under atmospheric air, both the resistance and the activation energy are substantially higher than in vacuum. After all, at temperatures exceeding 800 K, the buckypaper goes into reaction with oxygen from atmospheric air that results in its evaporation.

4. Conclusions

In agreement with previous measurements of the electrical transport mechanisms in mats consisting of SWNTs, the mixture of metallic and semiconducting tubes exhibits mixed temperature dependence of its resistance. Unlike others, however, we have represented the resistance using the model of the metallic and semiconducting terms connected in parallel rather than in series, which in particular enabled us to fit the resistance peak observed during recurrent heat treatment of the material. Another difference is that the semiconducting exponential decay fits the buckypaper resistance above the room temperature better than, for example, fluctuation-assisted tunneling or quasi-1D variable-range hopping observed in various fibrillar systems (polymers, nanotube mats). The simplest explanation is that either the latter mechanisms are inappropriate above room temperature or there are more fundamental structural differences between investigated materials (tube/bundle density, presence of defects, etc.), which are known to induce the bandgap in the tubes. Unfortunately, electrical conductivity mechanisms suffer from metastability, and another temperature-dependent terms need to be applied to the model as long as the buckypaper is subjected to thermal treatment.

Acknowledgment

Authors thank Mr. Z. Polakowski for his valuable technical support.

References

[1] Saito R, Fujita M, Dresselhaus G, Dresselhaus MS. Electronic structure of chiral graphene tubules. Appl Phys Lett 1992;60(18): 2204–6.

[2] Bradley K, Jhi SH, Collins PG, Hone J, Cohen ML, Louie SG, et al. Is the intrinsic thermoelectric power of carbon nanotubes positive? Phys Rev Lett 2000;85(20):4361–4.

[3] Zahab A, Spina L, Poncharal P, Marliere C. Water-vapor effect on the electrical conductivity of a single-walled carbon nanotube mat. Phys Rev B 2000;62(15):10000–3.

[4] Lee RS, Kim HJ, Fischer JE, Thess A, Smalley RE. Conductivity enhancement in single-walled carbon nanotube bundles doped with K and Br. Nature 1997;388(6639):255–7.

[5] Wei B, Spolenak R, Kohler-Redlich P, Ruhle M, Arzt E. Electrical transport in pure and boron-doped carbon nanotubes. Appl Phys Lett 1999;74(21):3149–51.

[6] McEven P, Bockrath M, Cobden DW, Yoon YG, Louie SG. Disorder pseudospins and backscattering in carbon nanotubes. Phys Rev Lett 1999;83(24):5098–101.

[7] Thess A, Lee R, Nikolaev P, Dai H, Petit P, Robert J, et al. Crystalline ropes of metallic carbon nanotubes. Science 1996;273(5274):483–7.

[8] Bethune DS, Klang CH, deVries MS, Gorman G, Savoy R, Vazquez J, et al. Cobalt-catalysed growth of carbon nanotubes with single-atomic-layer walls. Nature 1993;363(6430):605–7.

[9] Seraphin S, Zhou D. Single-walled carbon nanotubes produced at high yield by mixed catalysts. Appl Phys Lett 1994;64(16):2087–9.

[10] Yadaw T, Withers JC, Seraphin S, Wang S, Zhou D. Novel forms of carbon II. MRS Symp Proc 1994:275–82.

[11] Shi Z, Lian Y, Zhou X, Gu Z, Zhang Y, Ijima S, et al. Mass-production of single-wall carbon nanotubes by arc discharge method. Carbon 1999;37(9):1449–53.

[12] Rao AM, Richter E, Bandow S, Chase B, Eklund PC, Wiliams KA, et al. Diameter-selective Raman scattering from vibrational modes in carbon nanotubes. Science 1997;275(5297):187–91.

[13] Sheng P. Fluctuation-induced tunneling conduction in disordered materials. Phys Rev B 1980;21(6):2180–95.

[14] Pietronero L. Ideal conductivity of carbon π polymers and intercalation compounds. Synth Met 1983;8(3–4):225–31.

[15] Kaiser AB. Electronic transport properties of conducting polymers and carbon nanotubes. Rep Prog Phys 2001;64:1–49.

[16] Bernasconi J. Electrical conductivity in disordered systems. Phys Rev B 1973;7(6):2252–60.

[17] Rosenbaum TF, Andres K, Thomas GA, Lee PA. Conductivity cusp in a disordered metal. Phys Rev Lett 1981;46(8):568–71.

[18] Kaiser AB, Dusberg G, Roth S. Heterogeneous model for conduction in carbon nanotubes. Phys Rev B 1998;57(3):1418–21.

[19] Szroeder P, Electronic properties of carbon nanotubes, Nicholas Copernicus University, Toruń, Poland, Ph.D. Thesis, 2003.